2024 IFIP Networking Conference (IFIP Networking)

RM-Gen: Conditional Diffusion Model-Based Radio Map Generation for Wireless Networks

Xuanhao Luo, Zhizhen Li, Zhiyuan Peng, Dongkuan Xu, Yuchen Liu
North Carolina State University, USA

***Abstract*—Radio map is crucial for optimizing wireless network performance and configuration, aiding in tasks such as network planning, virtualization, and mobility management by providing a visual representation of radio-frequency signal strength in specific locations. However, generating precise radio maps with limited prior knowledge remains a significant challenge. Existing research in this field relies on extensive contextual information or computations, such as detailed geographic maps and exhaustive measurements. This hinders the adaptability of obtaining radio maps across varying network conditions and environmental changes. In this study, we explore the potential of generating radio maps using a generative diffusion probabilistic model, applicable to both indoor and outdoor wireless network scenarios. Specifically, we propose leveraging two accessible information pieces as input conditions for the generative model: sparse signal strength data and transmitter locations, respectively. This approach enables cost-effective radio map generation, particularly valuable in complex scenarios where obtaining comprehensive measurements is challenging. To ensure the training of the generative diffusion-based model for an adaptable map-based prediction, we develop a ray-tracing-based method to synthetically collect training data covering a wide range of fine-grained network scenarios across both 60 GHz and sub-6GHz frequency bands. Through comprehensive evaluations, we demonstrate the feasibility of our generative model to synthesize high-quality radio maps with only a small amount of measurement data or access point locations as guidance, achieving an accuracy rate of over 95% in various wireless network scenarios.**

***Index Terms*—Diffusion models, generative AI, radio map generation, wireless networks.**

I. Introduction

With the emergence of bandwidth-demanding applications such as virtual reality, video streaming and real-time communications, the demand for high-speed and reliable wireless networks is increasing. Millimeter-wave (mmWave) technology, particularly in the 60 GHz frequency band, is revolutionizing indoor wireless communication by offering significant advantages for dense, short-range networks. Concurrently, 5G technology is redefining outdoor cellular networks, enabling faster data speeds, reduced latency, and increased network capacity on a much broader scale. These advancements underscore the growing importance of efficient planning and timely deployment with upgraded network infrastructure. In such an evolving landscape of wireless networks, the radio map has emerged as a pivotal tool for optimizing network performance and configuration. A radio map is a graphical representation of received signal strength (RSS) at various location spots, offering a visual insight into the radio-frequency (RF) signal coverage and strength within a specific area. This detailed mapping facilitates the identification of strong and weak signal reception in any location of interest, thereby enabling targeted enhancement in network coverage and reliability.

In practice, the criticality of radio maps becomes increasingly evident due to their role in understanding wireless propagation characteristics, managing interference, planning capacity, and ensuring deployment efficiency. This enables network operators to strategically place base stations (BSs), configure antennas, and virtualize networks. Several typical recent application venues involve predictive resource planning [1], construction of digital twin networks [2], [3], and trajectory design for drone-assisted communications [4]. For instance, by providing detailed RSS information in spatial domain, network resources can be evenly allocated among areas with poor and strong connectivity, enabling ubiquitous and fair quality of user services. In the context of digitalizing the networks [2], radio maps, which carry abundant spatial RF data, facilitate the creation of accurate digital replicas of physical network attributes. This is crucial for simulating and analyzing what-if behavior under various channel conditions. Furthermore, the significance of radio maps is amplified in the studies of non-terrestrial networks, such as those utilizing unmanned aerial vehicles (UAVs) as mobile access points (APs) [4]. In such scenarios, the mapped RSS is used to determine optimal UAV trajectories that address network coverage gaps, especially in areas where traditional ground-based infrastructure is limited.

Despite the evident advantages and widespread applications, challenges persist in generating accurate and complete radio maps. Even minor alterations in the physical environment or the relocation of transmitters can result in significant fluctuations in radio maps, as illustrated in Fig. 1(a)-(c), with the RSS measurements of three distinct AP locations in an indoor wireless local-area network (WLAN). Consequently, collecting real-world data across all possible scenarios to obtain various radio maps is impractical due to the extensive measurement campaigns required. To address this issue, some interpolation-based algorithms have been adopted, such as Kriging [5], matrix completion [6], and dictionary learning [7]. However, these approaches often lack the ability to learn from experience, resulting in limited generalization capabilities, especially in dynamic and evolving network settings. With the advancement of artificial intelligence (AI), certain deep learning-based methods have been proposed to predict the entire radio map [8]–[10]. However, these methods typically rely on extensive environmental information, including detailed geographic maps and object parameters, which may not

978-3-903176-63-8/24/$31.00 ©2024 IEEE

always be readily available. These challenges highlight the necessity for a cost-effective approach to derive precise and adaptable radio maps with minimal prior knowledge, which is the focus of our research. Inspired by the remarkable success of generative AI techniques, particularly the effectiveness of diffusion probabilistic models in generating realistic images [11], [12], we are motivated to explore their potential for synthesizing radio maps in wireless networks. To this end, this work presents the following contributions:

- We propose *RM-Gen*, a conditional diffusion model-based framework, for generating radio maps across diverse wireless scenarios, including mmWave WLANs and 5G cellular networks, using sparse measurement data and environmental information. To the best of our knowledge, this is the first endeavor to leverage generative diffusion models for constructing radio maps in wireless networks.
- We demonstrate the feasibility of using two accessible information pieces as input conditions for the generative model: 1) a limited amount of RSS information and/or 2) transmitter locations. This approach facilitates the cost-effective generation of radio maps, especially useful in complex scenarios where obtaining comprehensive measurements is challenging.
- We develop a data collection method to synthetically generate high-quality training data covering a wide range of fine-grained network scenarios, which is then used to train the generative diffusion-based model for adaptable radio map prediction.
- We perform comprehensive evaluations using the two collected radio map datasets across both 60 GHz and sub-6GHz frequency bands. The results show that *RM-Gen* exhibits the capability to efficiently generate precise radio maps, achieving accuracy of over 95% in both indoor and outdoor wireless network scenarios.

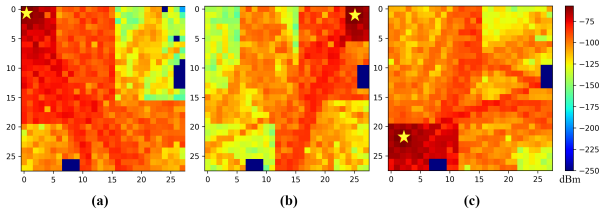

Fig. 1: Radio maps with different BS/AP locations (denoted by stars) in a mmWave network scenario.

II. Conditional Diffusion Model for Radio Map Generation

In this section, we first formulate the map generation problem as an optimization problem and propose a denoising diffusion probabilistic model as the solution, detailing the generation process based on different input information. Additionally, we introduce a map-based data collection method, which relies on radio frequency (RF)-based ray-tracing analysis.

A. Problem Formulation

In this work, the objective is to develop a generative model that can generate a complete radio map for an $N \times N$ area, leveraging a set of predefined conditions (prior knowledge) c. The conditions c consist of a set of parameters or contexts that serve as the input for our *RM-Gen*. These can include a small amount of measured RSS and transmitter (Tx) location, which are often easier to obtain in practice. In this way, such a map generation problem can be represented by a function $F : c \rightarrow \mathbb{R}^{N\times N}$, which takes the conditions c as input and outputs the estimated radio map, denoted as $\hat{M}$.

Specifically, the collected RSS information, referred to as partial RSS fragments, can be denoted as $\phi = \{\phi_1, \phi_2, \ldots, \phi_k\}$. In this situation, our task is to map ϕ to $\hat{M}$, which can be represented by the function $F_1 : \phi \rightarrow \mathbb{R}^{N\times N}$. On the other hand, the transmitter locations can be denoted as $Tx = \{Tx_1, Tx_2, \ldots, Tx_n\} = \{(x_1, y_1), (x_2, y_2), \ldots, (x_n, y_n)\}$; therefore, the task becomes mapping Tx to $\hat{M}$, represented as $F_2 : Tx \rightarrow \mathbb{R}^{N\times N}$.

With both types of conditions described above, the objective of our problem can be transformed to minimize the difference between the generated radio map $\hat{M}$ and the ground-truth radio map M, where $M \in \mathbb{R}^{N\times N}$ is based on empirical or measurement results. This difference can be quantified by $D(M, \hat{M})$, resulting in the following optimization problem:

$$\begin{aligned} &\min D(M, \hat{M}) \\ &\text{s.t. } D(M, \hat{M}) = \sum_{i=1}^{N}\sum_{j=1}^{N} |M_{ij} - \hat{M}_{ij}|, \end{aligned} \tag{1}$$

where $i = 1, 2, \ldots, N$ and $j = 1, 2, \ldots, N$ represent the rows and columns of grid Rx within the radio map, respectively. The optimal result can be achieved by iteratively training a generative diffusion model such that $\hat{M}$ closely aligns with M under a given set of conditions c.

B. Denoising Diffusion Probabilistic Models

In general, a diffusion model consists of two processes: a forward process and a reverse process. The forward process is a Markov chain that adds Gaussian noise at each time step. Let $q(x_0)$ be the RSS data distribution, the forward process can be defined as $q(x_t|x_{t-1})$, where $q(x_t)$ is the noisy map at time step t. The Gaussian noise added at each time step t is controlled by a variance schedule $\beta_1, \ldots, \beta_T$, where T is the total time step. Consequently, the forward process can be derived as:

$$q(x_{1:T}|x_0) = \prod_{t=1}^{T} q(x_t|x_{t-1}), \tag{2}$$

where

$$q(x_t|x_{t-1}) = \mathcal{N}(x_t; \sqrt{1-\beta_t}x_{t-1}, \beta_t\mathbf{I}). \tag{3}$$

During the diffusion process, $\beta_t \in (0, 1)$ always increases as t grows, i.e., $0 < \beta_1 < \beta_2 < \cdots < \beta_T < 1$. For $T \rightarrow \infty$, RSS data x_T will eventually approach an isotropic Gaussian distribution. At time step t, the noisy map x_t is

sampled from a conditional Gaussian distribution with a mean of $\mu_t = \sqrt{1-\beta_t}x_{t-1}$ and a variance of $\sigma_t^2 = \beta_t$, hence,

$$x_t = \sqrt{1-\beta_t}x_{t-1} + \sqrt{\beta_t}\epsilon, \tag{4}$$

where $\epsilon \sim \mathcal{N}(0, \mathbf{I})$. According to the property of Gaussian distribution, x_t can be sampled at an arbitrary time step t in a closed form, i.e.,

$$q(x_t|x_0) \sim \mathcal{N}(x_t; \sqrt{\bar{\alpha}_t}x_0, (1-\bar{\alpha}_t)\mathbf{I}), \tag{5}$$

where $\alpha_t := 1 - \beta_t$ and $\bar{\alpha}_t := \prod_{i=1}^{t} \alpha_i$. Then, x_t can be further formulated as:

$$x_t = \sqrt{\bar{\alpha}_t}x_0 + \sqrt{1-\bar{\alpha}_t}\epsilon. \tag{6}$$

In the reverse process, the diffusion model recovers $\mathbf{x_0}$ by denoising x_t. Such an reverse process can be defined as a Markov chain as:

$$p_\theta(x_{0:T}) := p(x_T)\prod_{t=1}^{T} p_\theta(x_{t-1}|x_t), \tag{7}$$

where $x_T \sim \mathcal{N}(\mathbf{0}, \mathbf{I})$, and $p_\theta(x_{t-1}|x_t)$ can be represented as:

$$p_\theta(x_{t-1}|x_t) := \mathcal{N}(x_{t-1}; \mu_\theta(x_t, t), \Sigma_\theta(x_t, t)). \tag{8}$$

Following the DDPM approach proposed in [11], it is proved that the reverse process can learn the mean value of $\mu_\theta(x_t, t)$. When setting $\Sigma_\theta(x_t, t) = \sigma_t^2\mathbf{I}$, where $\sigma_t^2 = \frac{1-\bar{\alpha}_{t-1}}{1-\bar{\alpha}_t}\beta_t$, $\mu_\theta(x_t, t)$ can be derived as:

$$\mu_\theta(x_t, t) = \frac{1}{\sqrt{\alpha_t}}\left(x_t - \frac{\beta_t}{\sqrt{1-\bar{\alpha}_t}}\epsilon_\theta(x_t, t)\right), \tag{9}$$

where ϵ_θ is the trainable denoising function estimating the noise vector in the reverse process. Based on this, we can formulate our loss function of the map generation model as:

$$\mathcal{L} = \mathop{\mathbb{E}}_{x_0\sim q(x_0),\epsilon\sim\mathcal{N}(0,\mathbf{I}),t} \|\epsilon_\theta(x_t, t) - \epsilon\|_2^2. \tag{10}$$

C. Conditional DDPM for Radio Map Generation

In our *RM-Gen*, the forward diffusion process is formulated with Eq. (2)-(6) as detailed in Sec. II.B. Considering the two conditions, i.e., partial RSS fragments and Tx locations, the objective is to train a generative model $p_\theta(x_0|e_\theta(c))$ capable of estimating the radio signal distribution $q(x_0)$, where e_θ represents the encoder used to extract the features of conditions c. As a result, the reverse process can be derived as:

$$p_\theta(x_{0:T}|e_\theta(c)) := p(x_T)\prod_{t=1}^{T} p_\theta(x_{t-1}|x_t, e_\theta(c)), x_T \sim \mathcal{N}(\mathbf{0}, \mathbf{I}), \tag{11}$$

$$p_\theta(x_{t-1}|x_t, e_\theta(c)) := \mathcal{N}(x_{t-1}; \mu_\theta(x_t, t|e_\theta(c)), \Sigma_\theta(x_t, t|e_\theta(c))). \tag{12}$$

As described in Sec. II.B, we have $\Sigma_\theta(x_t, t|e_\theta(c)) = \Sigma_\theta(x_t, t) = \sigma_t^2\mathbf{I}$, where $\sigma_t^2 = \frac{1-\bar{\alpha}_{t-1}}{1-\bar{\alpha}_t}\beta_t$. Hence, the diffusion model can learn the mean $\mu_\theta(x_t, t|e_\theta(c))$ represented as:

$$\mu_\theta(x_t, t|e_\theta(c)) = \frac{1}{\sqrt{\alpha_t}}\left(x_t - \frac{\beta_t}{\sqrt{1-\bar{\alpha}_t}}\epsilon_\theta(x_t, t|e_\theta(c))\right) \tag{13}$$

Next, the reverse process of our conditional DDPM turns to train ϵ_θ by minimizing the following loss function based on Eq. (10):

$$\mathcal{L} = \mathop{\mathbb{E}}_{x_0\sim q(x_0),\epsilon\sim\mathcal{N}(0,\mathbf{I}),t} \|\epsilon_\theta(x_t, t|e_\theta(c)) - \epsilon\|_2^2 \tag{14}$$

Lastly, to predict the noise vector ϵ in the reverse process, the denoising function $\epsilon_\theta(x_t, t|e_\theta(c))$ is realized by training a U-Net [13]. The detailed diffusion model framework of our *RM-Gen* is shown in Fig. 2.

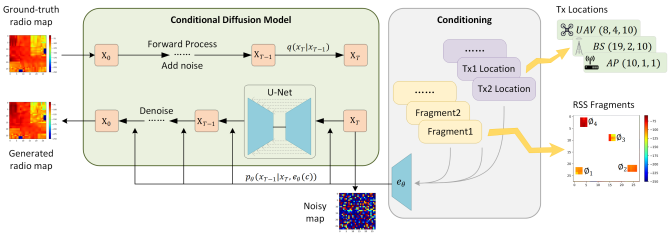

Fig. 2: Overview of our conditional diffusion model *RM-Gen*.

D. Map-based Data Collection with Ray-tracing Analysis

To augment the map-based RSS dataset for training our diffusion model, we utilize the commercial ray tracer *Wireless Insite*® [1] to synthetically generate radio map datasets in both indoor mmWave and an outdoor sub-6GHz network scenarios. Specifically, for the mmWave dataset, we focus on the 60 GHz frequency band. In this context, arbitrary 3-D indoor scenarios can be configured, such as an office/lab environment layout with dimensions of 14m $\times$ 14m $\times$ 3m as depicted in Fig. 3(a). These indoor scenarios can include various objects such as wooden chairs, glass tables, and wooden cabinets. The AP serves as the transmitter and can be deployed at arbitrary location to emit signals. To obtain the entire radio map, we meticulously divide the space into a number of small grids and deploy a client receiver (Rx) every 0.5m to capture the intricate details of 60 GHz signal propagation and attenuation. Next, the ray-tracing analysis simulates the propagation of electromagnetic waves by tracing the paths of individual rays as they interact with surfaces and objects within the environment. Finally, the received signal strength at each Rx is calculated based on the contributions of all traced rays, accounting for their intensities, phases, and arrival times. This process allows us to effectively collect $\sim$ 30,000 radio maps with different scenario configurations, offering invaluable insights into the behavior of 60 GHz mmWave communications within a controlled setting.

For the sub-6GHz network dataset, we construct 3-D square outdoor open scenarios, as depicted in Fig. 3(b), which include features such as the ocean (blue region), the beach (light green region), the land (dark green region), and various buildings of different sizes and heights. Similar to the mmWave data collection, BSs operating at a frequency of 3.7 GHz can be randomly deployed in the scenario. This frequency band is

[1]https://www.remcom.com/wireless-insite-em-propagation-software

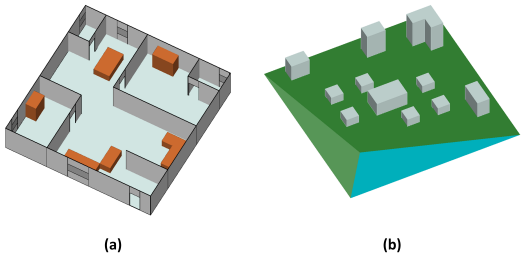

Fig. 3: 3-D scenario layout of (a) an indoor scenario and (b) an outdoor scenario.

chosen to align with standard 5G frequency bands and to ensure realistic simulation of outdoor cellular networks. Considering the longer-range propagation of sub-6GHz signals, the grid-based Rx are deployed at intervals of every 10 meters within the environment. Overall, approximately 26,000 radio maps are collected in such outdoor network scenarios. For simplicity, we denote the above two datasets as **RM-In** and **RM-Out**, respectively. It is worth noting that the ray-tracing technique is often used to estimate ground-truth data on RSS for different locations in each data set instance. Measurement studies have demonstrated that the signal profiles produced by ray-tracing techniques are quite close to real measurements in various wireless scenarios [14], [15].

III. Performance Evaluation

To evaluate the effectiveness of our proposed *RM-Gen*, we conduct extensive evaluations using two collected datasets. In the following sections, we begin by demonstrating the efficacy of our core generative module, DDPM. Subsequently, we evaluate the performance of *RM-Gen* using partial RSS fragments and Tx locations as the input condition, respectively.

A. Performance of DDPM

We divide the experimental settings into two parts. In the first part, partial RSS fragments are used as conditions to generate full radio maps, and in the second part, we use Tx locations as conditions for training DDPM. As describe in Sec. II, the forward process adds noise to the initial map according to the variance schedule β over T time steps. For our evaluations, we set $T = 400$ time steps, and the variance increases linearly from $\beta_1 = 10^{-4}$ to $\beta_T = 0.02$. To train the diffusion model generating radio maps using the measured RSS data pieces, we set a learning rate $\gamma = 10^{-4}$ and employ Adaptive Moment Estimation (Adam) to adjust γ for a total of 100 epochs. The training loss curve for this setup on the RM-In dataset, depicted in Fig. 4(a), demonstrates a consistent decrease in loss value over iterations, indicating an improvement in the model's accuracy during noise prediction.

In the second part, we utilize Tx locations as conditions to generate radio maps. We set the learning rate $\gamma = 10^{-5}$ and use Adam to adjust γ across 50 epochs. Fig. 4(b) illustrates the training loss curve for this scenario on the RM-In dataset, where a similar trend of decreasing loss values suggests the model's noise prediction capability. Comparing the loss curves in Fig. 4(a) and Fig. 4(b), it can be observed that the performance using Tx locations as the condition tends to converge around 0.02, whereas the curve with partial RSS fragments as the condition converges closer to 0.01. This observation aligns with subsequent evaluation results, indicating that the DDPM trained with partial RSS fragments are more adept at predicting noise and therefore, it can generate more accurate radio maps. For the RM-Out dataset, the trend of loss curve for the two experiments is similar to the loss curve on RM-In dataset, which is omitted here due to space constraints.

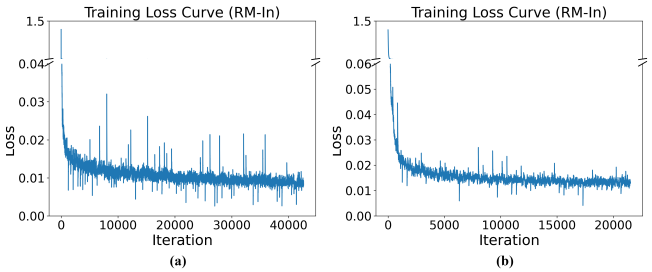

Fig. 4: Model loss curve using (a) partial RSS fragments and (b) Tx locations as conditions.

B. Radio Map Generation with RSS Fragments

To demonstrate the effectiveness using *RM-Gen* in generating radio maps, we first evaluate the model performance using partial RSS fragments as the prior knowledge, which then gradually compensates for the missing segments to form a complete radio map. Fig. 5 shows the accuracy of generated radio maps from *RM-Gen* in both indoor mmWave and outdoor sub-6GHz networks under varying error tolerance rates (ETRs). The ETR is a metric that specifies the maximum allowable percentage difference between the RSS values in a generated radio map and those in a ground-truth radio map. For instance, an ETR of 0.10 implies that a performance difference ratio of 10% is acceptable, and a lower ETR indicates more stringent criteria for the quality of the radio map.

We conduct experiments with varying percentages of known RSS fragments, ranging from 5% to 15%, to examine their impact on the accuracy of the generated radio maps. In Fig. 5(a), concerning indoor mmWave scenarios, there is a noticeable trend of improved performance with increasing fragment percentages across all ETRs. This suggests that utilizing more data pieces enhances the model's capability to generate accurate radio maps. Additionally, the generation performance consistently improves as the ETR increases. This correlation is expected, as a higher tolerance for error typically corresponds to higher accuracy. It is worth noting that when ETR is 0.10, the accuracy with all three fragment percentages exceeds 95%, highlighting *RM-Gen*'s efficiency in generating precise radio maps even with just 5% measured RSS data.

Contrastingly, in Fig. 5(b), illustrating the generation performance in outdoor cellular network scenarios, while the model exhibits a similar trend, its performance is comparatively lower. For instance, at ETR = 0.10, the accuracy is around

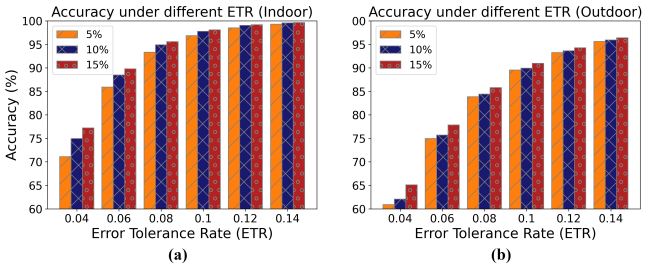

Fig. 5: Generation accuracy using partial RSS fragments for (a) indoor mmWave WLANs and (b) sub-6GHz outdoor networks.

90%, which is over 5% lower than the evaluated cases in Fig. 5(a). This difference can be attributed to the complexity of scenarios as well as the inherent characteristics of mmWave and sub-6GHz signals. Outdoor network settings are typically larger than indoor scenarios and include more complex elements like buildings. Additionally, sub-6GHz signals, commonly used in outdoor environments, penetrate obstacles more effectively, resulting in more irregular RSS distributions and posing a greater challenge for accurate generation.

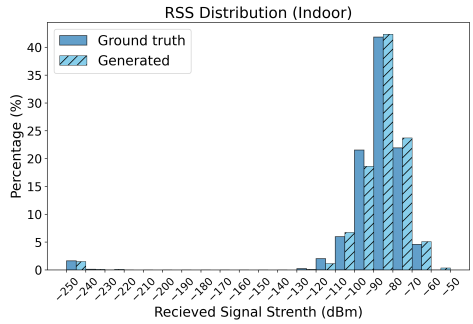

Fig. 6: RSS distribution for indoor mmWave WLANs.

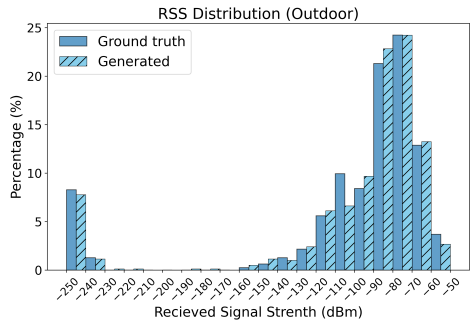

Fig. 7: RSS distribution for outdoor sub-6GHz networks.

To further explore such differences between mmWave and sub-6GHz signals, we randomly select two samples from the indoor and outdoor radio maps generated by *RM-Gen* and zoom in on the data results. Fig. 6 and Fig. 7 depict the RSS distribution between the generated radio maps and the ground truths for these samples. As seen in Fig. 6, the RSS values in indoor mmWave scenarios cover a wide range from -250 dBm to -50 dBm, with a concentration between -100 dBm and -70 dBm. Notably, the RSS between -80 dBm and -90 dBm accounts for the highest proportion with a clear peak, representing more than 40% of the RSS distribution. Conversely, Fig. 7 illustrates that outdoor cases, while covering a similar range, exhibit a more uniform distribution, primarily between -120 dBm and -60 dBm. In particular, the peaks for outdoor sub-6GHz RSS, situated between -90dBm and -70dBm, are more dispersed than indoor mmWave RSS, reflecting the variability and instability of the outdoor radio profiles.

Besides these observations that underscore the distinct propagation characteristics of indoor mmWave and outdoor sub-6GHz signals, the results reveal that the RSS distribution of our generated samples closely aligns with the ground-truth results, affirming the *RM-Gen*'s capability to accurately synthesize radio maps in varying scenarios.

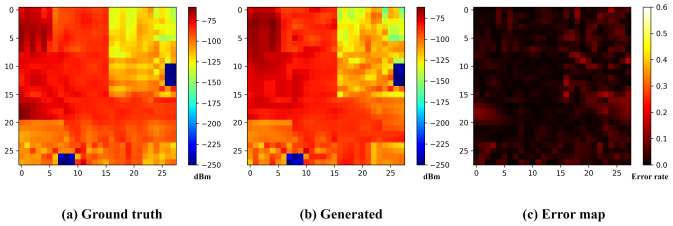

Fig. 8: Visualization of generated radio maps for indoor cases.

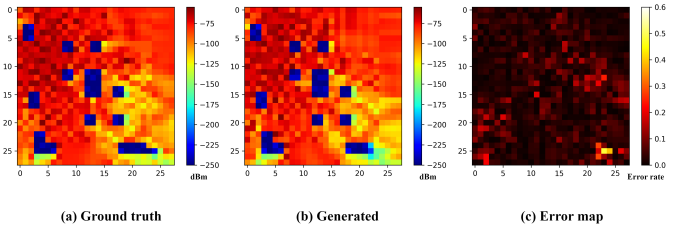

Fig. 9: Visualization of generated radio maps for outdoor cases.

We also provide visual representations of the generation results from *RM-Gen*. Specifically, Figs. 8(a)-(b) show a ground-truth radio map and a corresponding generated radio map with the 10% RSS fragments, respectively, while Fig. 8(c) illustrates the error map between them. When considering the environment configuration depicted in Fig. 3(a), it is notable that both radio maps shown in Figs. 8(a)-(b) exhibit similar trends when examining each isolated area within the scenario. Moreover, Fig. 8(c) indicates that the error rate in most regions is less than 0.1, affirming the accuracy of generated radio map.

Likewise, Fig. 9 shows the generation results for an outdoor network scenario, demonstrating a high alignment between the generated radio map and the ground-truth radio map. However, upon comparing the error maps from Fig. 8(c) and Fig. 9(c), it is evident that the outdoor scenario exhibits more "polluted" points with higher error rates. This finding is consistent with

our previous evaluation results that RM-Gen performs better in generating indoor radio maps.

C. Radio Map Generation with Tx Locations

In addition to using partial RSS fragments, we investigate the feasibility of employing only Tx locations as input conditions to RM-Gen in radio map generation. The conditional diffusion model is trained with two Tx locations as input on the RM-In and RM-Out datasets, and the results reported in Fig. 10. It is observed that as the ETR increases, the generation accuracy improves in both indoor and outdoor network scenarios. Notably, the model performs significantly better in indoor scenarios than in outdoor scenarios. This result is consistent with our observation in Sec. III.B. Particularly, when comparing the generation accuracy depicted in Fig. 5, the results are notably inferior when Tx locations are employed as conditions compared to RSS fragments. Specifically, at ETR=0.10, it achieves accuracies of only 81.95% and 74.26% in indoor and outdoor network scenarios, respectively. The reduced accuracy observed when employing Tx locations as conditions is attributed to the limited information they convey compared to RSS fragments. While RSS fragments offer rich local features of signal distributions, Tx location data primarily provides signaling source information, posing challenges for accurately reconstructing full radio maps. However, despite these limitations, utilizing Tx location as conditions presents intriguing practical potential. Generating radio maps based on planned BS/AP positions can be particularly advantageous in contexts where performing measurements or ray-tracing analysis is impractical or costly. Future research could focus on enhancing the model's ability to interpret and effectively utilize Tx location information alongside sparse RSS measurements.

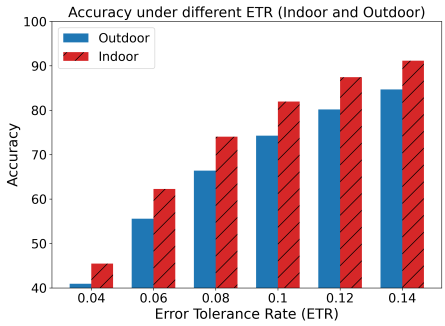

Fig. 10: Generation accuracy using Tx locations as condition.

IV. Conclusion

This study introduced *RM-Gen*, a conditional diffusion model designed for radio map generation in wireless networks. Leveraging generative AI techniques, *RM-Gen* efficiently synthesizes accurate radio maps using limited and accessible prior data, thereby contributing to various network tasks such as BS/AP planning and digital twinning. The results showcased the remarkable accuracy of the generated radio maps, achieving accuracy rates of 95% for indoor WLANs and 90% for outdoor cellular networks across various ETRs. This performance underscores not only the feasibility of generative AI techniques in RF signal analysis but also their practical applicability in diverse network contexts. Future research endeavors may involve exploring the combined conditioning data and optimal fragment selection techniques to further enhance the predictive capability of generative models.

Acknowledgment

This research was supported by the National Science Foundation through Award CNS–2312138.

References

[1] Phillips, Caleb, Douglas Sicker, and Dirk Grunwald. "A survey of wireless path loss prediction and coverage mapping methods." *IEEE Communications Surveys & Tutorials* 15, no. 1 (2012): 255-270.

[2] Almasan, Paul, Miquel Ferriol-Galmés, Jordi Paillisse, José Suárez-Varela, Diego Perino, Diego López, Antonio Agustin Pastor Perales et al. "Network digital twin: Context, enabling technologies, and opportunities." *IEEE Communications Magazine*, no. 11 (2022): 22-27.

[3] Z. Yang, M. Chen, Y. Liu, and Z. Zhang, "A joint communication and computation framework for digital twin over wireless networks", *IEEE Journal of Selected Topics in Signal Processing (JSTSP)* [J], 2024.

[4] Li, Ke, Xu Zhu, Yufei Jiang, and Fu-Chun Zheng. "Closed-form beamforming aided joint optimization for spectrum-and energy-efficient UAV-BS networks." *In 2019 IEEE Global Communications Conference (GLOBECOM)*, pp. 1-6. IEEE, 2019.

[5] Sato, Koya, and Takeo Fujii. "Kriging-based interference power constraint: Integrated design of the radio environment map and transmission power." *IEEE Transactions on Cognitive Communications and Networking 3*, no. 1 (2017): 13-25.

[6] Sun, Hao, and Junting Chen. "Propagation map reconstruction via interpolation assisted matrix completion." *IEEE Transactions on Signal Processing* 70 (2022): 6154-6169.

[7] Kim, Seung-Jun, and Georgios B. Giannakis. "Cognitive radio spectrum prediction using dictionary learning." *In 2013 IEEE Global Communications Conference (GLOBECOM)*, pp. 3206-3211. IEEE, 2013.

[8] Levie, Ron, Çağkan Yapar, Gitta Kutyniok, and Giuseppe Caire. "RadioUNet: Fast radio map estimation with convolutional neural networks." *IEEE Transactions on Wireless Communications* 20, no. 6 (2021).

[9] Gupta, Ankit, Jinfeng Du, Dmitry Chizhik, Reinaldo A. Valenzuela, and Mathini Sellathurai. "Machine learning-based urban canyon path loss prediction using 28 ghz manhattan measurements." *IEEE Transactions on Antennas and Propagation* 70, no. 6 (2022): 4096-4111.

[10] Zhang, Songyang, Achintha Wijesinghe, and Zhi Ding. "RME-GAN: A Learning Framework for Radio Map Estimation based on Conditional Generative Adversarial Network." *IEEE Internet of Things Journal* (2023).

[11] Ho, Jonathan, Ajay Jain, and Pieter Abbeel. "Denoising diffusion probabilistic models." *Advances in neural information processing systems* 33 (2020): 6840-6851.

[12] Rombach, Robin, Andreas Blattmann, Dominik Lorenz, Patrick Esser, and Björn Ommer. "High-resolution image synthesis with latent diffusion models." *In Proceedings of the IEEE/CVF conference on computer vision and pattern recognition*, pp. 10684-10695. 2022.

[13] Ronneberger, Olaf, Philipp Fischer, and Thomas Brox. "U-net: Convolutional networks for biomedical image segmentation." *In Medical Image Computing and Computer-Assisted Intervention–MICCAI 2015: 18th International Conference*, Munich, Germany, October 5-9, 2015, Proceedings, Part III 18, pp. 234-241. Springer International Publishing, 2015.

[14] C. Wang, J. Huang, H. Wang, X. Gao, X. You, and Y. Hao, "6G wireless channel measurements and models: Trends and challenges". *IEEE Vehicular Technology Magazine*, 2020, 15(4), 22-32.

[15] B. Neekzad, K. Sayrafian-Pour, J. Perez, and J. S. Baras, "Comparison of ray tracing simulations and millimeter wave channel sounding measurements", *Proc. of IEEE Int'l Symposium on Personal, Indoor, and Mobile Radio Communications*, 2007.